Infrared Spectra of Nickel Octaethylporphyrin and Its Isotopomers Computed via Density Functional Theory−Scaled Quantum Mechanical (DFT−SQM) Method

Lindy K. Stoll,[†] Marek Z. Zgierski,[‡] and Pawel M. Kozlowski*[,†]

Department of Chemistry, University of Louisville, Louisville, Kentucky 40292, and Steacie Institute for Molecular Science, National Research Council of Canada, Ottawa, Ontario K1A OR6, Canada

Received: November 8, 2002

Gradient-corrected density functional theory (DFT) calculations were carried out to develop a scaled quantum mechanical (SQM) force field for nickel octaethylporphyrin (NiOEP). Frequencies for all vibrations were calculated for several conformers and isotopomers of NiOEP. Assignments of infrared active vibrations were made upon the basis of normal coordinate analysis of the resulting DFT−SQM force field. The spectra and vibrational assignments agree well with previously reported experimental infrared data for NiOEP, with only eight of the peaks in the simulated natural abundance spectrum being more than 10 cm^{-1} apart from their counterparts on the experimental natural abundance spectrum. Theoretically calculated isotopic shifts on simulated spectra resemble isotopic shifts observed experimentally. All but four shifts in the simulated meso-deuterated spectrum are within the same order of magnitude and in the same direction as those reported for experimental meso-deuteration, and none of the simulated ^{15}N shifts were more than 2 cm^{-1} larger or smaller than their respective experimental shifts.

Introduction

Vibrational spectroscopy, in particular resonance Raman (RR) spectroscopy, is one of the principal experimental techniques used to study biologically important porphyrins.[1] Vibrational spectra provide rich and unique fingerprints of metalloporphyrins, but the information contained in the spectra is not easily deciphered. The main shortcoming of vibrational spectroscopy is that its results have been traditionally difficult to interpret without guidance from normal coordinate analysis. A primary tool for the interpretation of metalloporphyrin vibrational spectra is the determination of the vibrational force field (FF), which is the potential energy surface as a function of the molecular geometry, and the subsequent normal coordinate analysis.

Before modern density functional theory (DFT) became capable of handling complex systems resembling the active site of metalloenzymes, such as metalloporphyrins, the development of vibrational force fields was carried out through empirical approaches. Nickel octaethylporphyrin, NiOEP (Figure 1), has been used by many researchers as a primary model for the development of an empirical force field for metalloporphyrins.[2,3] Studies by Kitagawa and co-workers on NiOEP and various isotopomers allowed them to make vibrational assignments for particular in-plane vibrations of the porphyrin skeleton.[2] Additionally, they were able to identify a number of overtones and combination bands. Later work by Spiro and co-workers extended the empirical force field and improved its quality.[3] The result was the development of a consistent porphyrin force field that enabled the assignment of all in-plane vibrations,[3a,3b] as well as an attempted characterization of out-of-plane vibrations.[3c] The empirical force field for NiOEP was later used as a guide in making vibrational assignments for cytochrome *c*[4a] and myoglobin.[4b]

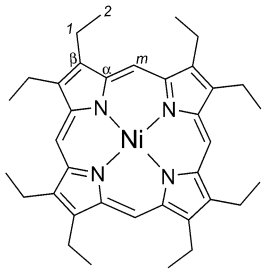

Figure 1. Structure of nickel octaethylporphyrin and its carbon atom labeling scheme.

Over the past few years, DFT calculations have become a powerful tool for developing force fields and assigning vibrations for relatively large systems such as metalloporphyrins. The DFT approach represents substantial improvement over the earlier empirical force fields as shown in DFT studies of nickel porphine (NiP)[5a] and nickel tetraphenylporphyrin (NiTPP).[5b] In similar fashion, we have employed DFT in the analysis of NiOEP. Previously, we compared the results of DFT calculations for NiOEP with published experimental X-ray crystallography data.[6] This work presents simulated infrared (IR) spectra from DFT calculations and compares these simulated spectra with their experimental counterparts published earlier by Kincaid and co-workers.[7] A vibrational analysis of Raman-active vibrations will be presented in future publication.[8]

Computational Methods

Calculations reported in this paper were carried out using gradient-corrected density functional theory (DFT) with the Becke−Lee−Yang−Parr composite exchange correlation functional (B3LYP) as implemented in the Gaussian 98[9] suite of programs for electronic structure calculations. The B3LYP level of theory with 6-31G(d) [for H, C, and N atoms] and Ahlrichs VTZ (for Ni)[10] basis sets, successfully used in previous

* To whom correspondence should be addressed. E-mail: pawel@louisville.edu.
[†] University of Louisville.
[‡] National Research Council of Canada.

10.1021/jp022398m CCC: $25.00
Published on Web 04/24/2003

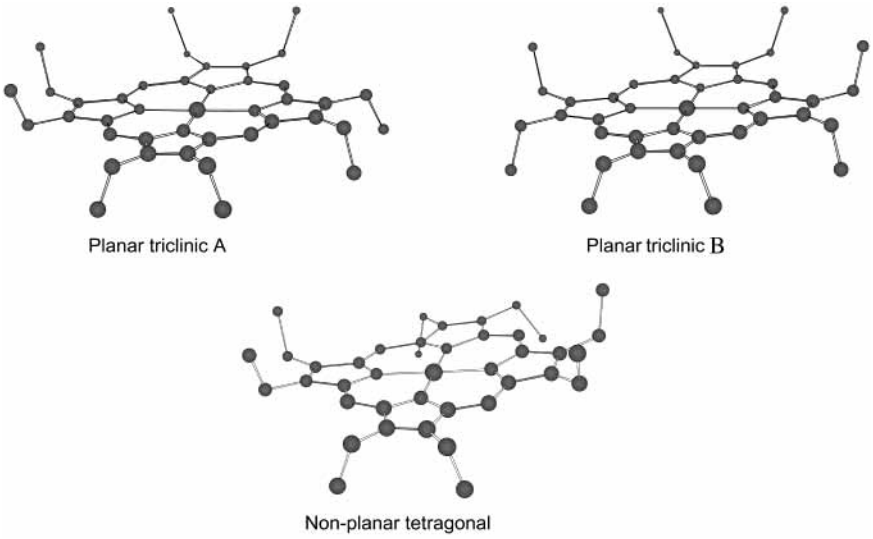

Figure 2. Structures of NiOEP conformers showing the orientation of the ethyl substituent groups.

TABLE 1: Scaling Factors as Applied to Force Constants

coordinate type	scaling factor[a]
X−Y stretch stretch between two non-hydrogen atoms)	0.9337
C−H stretch	0.9122
torsional bending	0.9619
XY−Z bend bend between three non-hydrogen atoms)	0.9880
XY−H bend in-plane bending of hydrogen atom)	0.9340
out-of-plane modes	0.9486

[a] The values used for scaling factors were optimized on free base porphine and its isotopomers as given in Kozlowski, P. M.; Jarzecki, A. A.; Pulay, P. *J. Phys. Chem.* **1996**, *100*, 7007. The scaling factors were used for NiOEP without additional optimization as in the NiP and NiTPP studies.

calculations on metalloporphyrins,[5,11] was employed in the present study. Cartesian force constants were calculated at the optimized geometry and then transformed to natural internal coordinates.[12] The natural internal coordinates were automatically generated by the TX90 program[13] and manually augmented. To refine the calculated DFT force constants, we used scaled quantum mechanical (SQM) procedure and scaled the resulting force constants according to the formula $F_{ij}' = (\lambda_i\lambda_j)^{1/2}F_{ij}$.[14] Force constants were scaled by applying scaling factors as given in Table 1 prior to vibrational analysis and creation of simulated spectra. No further optimization was performed after the scaling of the force constants. The program Molekel[15] was used for graphic visualization of vibrations.

Results and Discussion

X-ray crystallography data has been reported for three conformers of NiOEP: tetragonal, triclinic A, and triclinic B (Figure 2). These conformers differ principally by the orientation of the ethyl groups with respect to the porphyrin macrocycle. The X-ray data show the nonplanar tetragonal conformer to have S_4 symmetry and the triclinic A and triclinic B forms, which are planar, both to have C_{2h} symmetry. As reported previously,[6] DFT energy calculations on three conformers having structures similar to those studied crystallographically and on nonplanar (ruffled) versions of the triclinic A and triclinic B conformers reveal two important points. First, the ruffled versions of the two triclinic conformers are about 0.2 kcal/mol lower than their planar counterparts. Second, the calculated energies for the nonplanar triclinic conformers and the tetragonal conformer, which is also nonplanar, are essentially degenerate, being within 0.09 kcal/mol of each other. The small energy difference between conformers explains why a mixture of conformers is possible in NiOEP solutions and gas-phase NiOEP; however, the energy barrier between changes from one conformer to another is large enough that three distinct conformers have been crystallized successfully.

To understand better the characteristics of various conformers with respect to ethyl orientation and macrocycle planarity, infrared spectra were simulated from calculated frequencies and intensities for the tetragonal, ruffled and planar triclinic A, and ruffled and planar triclinic B conformers of NiOEP.

Kincaid and co-workers[7] published high-quality infrared spectra acquired in an argon matrix for both natural abundance NiOEP and its meso-deuterated analogue (NiOEP-d_4). A comparison of the experimental natural abundance NiOEP IR spectrum with the spectrum simulated from DFT calculations is presented in section A that follows, and a similar comparison for meso-deuterated NiOEP is discussed in section B. In section C, the effect of isotopic substitutions on simulated spectra is analyzed through comparison of the simulated natural abundance NiOEP spectrum with the simulated Ni-^{15}N-OEP, NiOEP-d_4, and NiOEP-d_{16} spectra.

A. Experimental and Simulated Natural Abundance Spectra. Though the simulated natural abundance spectra for the various conformers are all similar to the published experimental natural abundance spectrum for NiOEP collected in an argon matrix, none of them match perfectly. This was not unexpected because uncrystallized samples of NiOEP are thought to contain a mixture of conformers. Of the simulated spectra, the spectrum for the tetragonal conformer appears to be the one that is most similar to experimental spectra. As evidenced in Figure 3, there is good agreement overall between the simulated and the experimental spectra. Only eight of the peaks on the simulated spectrum are more than 10 cm^{-1} apart from their counterparts on the experimental spectrum. Intensities of the peaks also match reasonably well between the two spectra.

Table 2 presents data for the various spectra. Included in this table are the descriptions of vibrations as reported by Kincaid et al.[7] and descriptions that we propose. Vibrational assignments (ν_i, γ_j) are also presented in Table 2, and all reassignments from those proposed by Li et al.[3b] or Kincaid et al.[7] are noted. A complete vibrational assignment and detailed description of

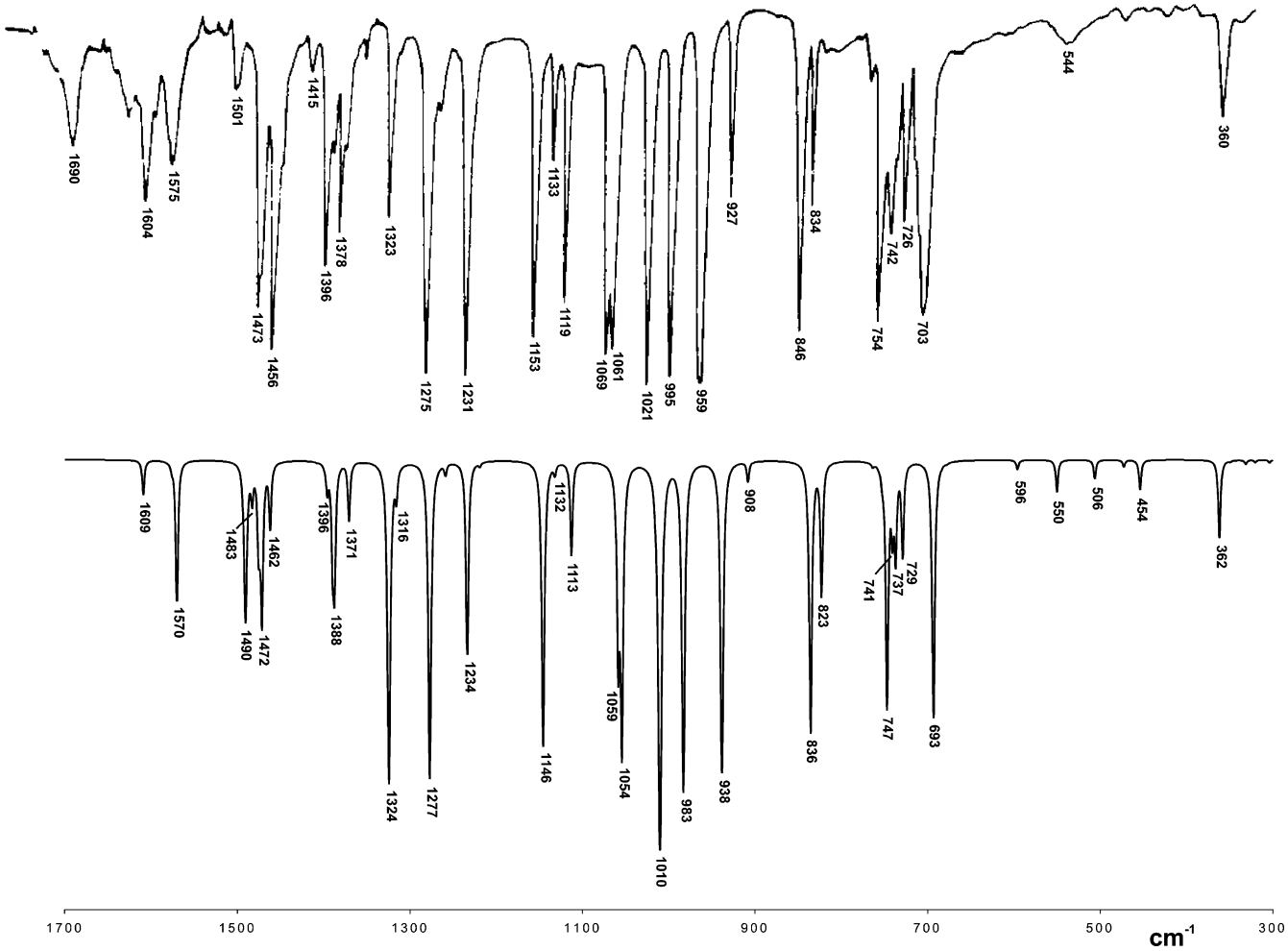

Figure 3. Comparison of experimental infrared spectrum (reproduced with permission from ref 7) with simulated spectrum (tetragonal conformer) for natural abundance NiOEP.

skeletal vibrations for NiOEP will be presented in a forthcoming publication.[8] Descriptions and assignments for peaks in the simulated spectra were made using information from the total energy distribution among the internal coordinates for each vibration and by observing the vibrations within graphical visualization software. The terminology used in describing the vibrations is in keeping with that used by Kincaid and co-workers,[7] such that the symbols ν, δ, and π refer to stretching, in-plane bending, and bending out of plane, respectively. The carbon atom labeling scheme is given in Figure 1, with the C_s atom of the experimental descriptions being equivalent to the C_1 (methylene carbon) atom shown in Figure 1 and used in the descriptions for peaks on the simulated spectra. The designations given for each frequency are arranged in approximate order of decreasing contribution.

In general, the descriptions presented in this paper agree with those given by Kincaid et al.,[7] the exceptions being those for the peaks with experimental wavenumbers 1690, 1275, 996, and 726 cm^{-1}. The peak seen in the experimental spectrum at 1690 cm^{-1} did not appear in our simulated spectra for any of the conformers and is now believed to be the result of impurities in the experimental sample.[16] Kincaid et al.[7] described the peak appearing at 1275 cm^{-1} as stretching of the $C_\alpha-C_\beta$ and $C_\beta-C_s$ bonds, but according to our data this peak, which appears at 1277 cm^{-1} on the simulated spectrum, is due mainly to vibrations of the ethyl constituents with some contribution from $\nu(C_\alpha C_\beta)$. The peak at 996 cm^{-1} (experimental)/983 cm^{-1} (simulated), vibration ν_{45}, was assigned originally to stretching of the $C_\alpha-N$ and $C_\alpha-C_m$ bonds, but our analysis indicated that this peak results from stretching of the $C_\alpha-C_\beta$ and $C_\alpha-N$ bonds and from a strong ethyl component, namely, the stretching of the C_1-C_2 bonds. Originally described as stretching of $C_\alpha-N$ bonds, the peak at 726 cm^{-1} (experimental)/729 cm^{-1} (simulated), vibration γ_{21}, appears instead to be due to out-of-plane vibrations of the porphyrin macrocyle [π(skeletal)]. This particular out-of-plane vibration, however, significantly displaces the nitrogen atoms with respect to the plane of the porphyrin macrocycle. This displacement may give rise to the appearance of a $\nu(C_\alpha N)$ component in experimental isotopic evaluation, which we believe to be the basis for the original description of this vibration as $\nu(C_\alpha N)$.

B. Experimental and Simulated Meso-Deuterated Spectra. A spectrum for the tetragonal conformer of NiOEP deuterated at the four C_m atoms, called meso-deuterated NiOEP or NiOEP-d_4, was simulated for comparison with the NiOEP-d_4 spectrum obtained by Kincaid and co-workers[7] (Figure 4). Table 2 gives values for the shifts reported by Kincaid et al.[7] and for the shifts that we observed in the simulated NiOEP-d_4 spectrum. Considering the spectrum as a whole, deuteration can shift each fundamental frequency only to lower values. Seemingly positive shifts result from a crossover in the assignment of individual modes. In general, the shifts observed in the simulated spectra resemble those reported for the experimental spectra. The 1501 cm^{-1} peak (ν_{39}) on the experimental spectrum shifts down to

TABLE 2: Frequencies (cm^{-1}) from Experimental and Simulated Spectra of NiOEP

experimental spectra[a]				simulated spectra									
na	Δd_4	Δ ^{15}N	description	S_4	Δd_4	Δd_{16}	Δ ^{15}N	$A_{ruffled}$	A_{planar}	$B_{ruffled}$	B_{planar}	assignment	description
1604			$\nu(C_\beta C_\beta)$	1609	6	4	−1	1606	1610	1606	1611	ν_{37}[b]	$\nu(C_\beta C_\beta)$, $\nu(C_\alpha C_m)$
1575	9	0	$\nu(C_\alpha C_m)$	1570	11	3	0	1567	1572	1567	1572	ν_{38}[b]	$\nu(C_\alpha C_m)$, $\nu(C_\beta C_\beta)$
1501	7	0	$\nu(C_\alpha C_m)$	1483	−2	−4	0	1483	1483	1483	1485	ν_{39}	ethyl, $\nu(C_\alpha C_m)$
1473	0	0	ethyl	1490	0	7	0	1491	1491	1491	1492		ethyl
1456	1	0	ethyl	1472	0	1	0	1472	1472	1473	1473		ethyl
				1462	0	373	0	1463	1462	1463	1463		ethyl
1396	4	0	$\nu(C_\alpha C_\beta)$, $\nu(C_\beta C_s)$	1396				1397	1397	1397	1397	ν_{40}	$\delta(C_\alpha C_m H)$, $\nu(C_\alpha N)$, $\nu(C_\alpha C_\beta)$, ethyl, $\nu(C_\beta C_1)$
				1388	0	0	0	1390	1390	1392	1391		ethyl
1378	−2	0	ethyl	1371	0		0	1371	1372	1371	1371	ν_{41}[c]	ethyl, $\nu(C_\beta C_1)$, $\nu(C_\alpha C_\beta)$
1323	1	0	ethyl	1324	−1	255	0	1325	1325	1325	1325		ethyl
				1316	0	347	0	1315	1315	1315	1316		ethyl
1275	8	0	$\nu(C_\alpha C_\beta)$, $\nu(C_\beta C_\beta)$	1277	9	457	0	1278	1278	1276	1276		ethyl, $\nu(C_\alpha C_\beta)$
1231	46	3	$\nu(C_\alpha C_m)$, $\nu(C_\alpha N)$, $\delta(C_\alpha C_m H)$	1234	282	−9	4	1235	1234	1233	1234	ν_{42}	$\delta(C_\alpha C_m H)$, $\nu(C_\alpha N)$, $\nu(C_\alpha C_\beta)$
1153	205	8	$\nu(C_\alpha N)$, $\delta(C_\alpha C_m H)$	1146	2	−53	6	1146	1145	1146	1145	ν_{44}[d]	$\nu(C_\beta C_1)$, $\nu(C_\alpha N)$, ethyl, $\delta(C_\alpha C_m H)$
1133	−18	12		1132	−52	29	10	1134				ν_{43}[d]	$\nu(C_\alpha N)$, $\delta(C_\alpha C_m H)$, $\nu(C_\beta C_1)$
1119	−2	2	ethyl	1113	−2	475	0	1113	1113	1113	1113		ethyl
1069	0	0	ethyl	1059	0	31	0	1059	1059	1064	1064		ethyl
1061	−1	0	ethyl	1054	−1	41	0	1056	1056	1056	1055		ethyl
1021	−3	0	ethyl	1010	−3	−99	2	1011	1010	1011	1011		ethyl, $\nu(C_\alpha C_\beta)$
996	0	5	$\nu(C_\alpha N)$, $\nu(C_\alpha C_m)$	983	3	140	5	984	984	984	984	ν_{45}	ethyl, $\nu(C_\alpha N)$, $\nu(C_\alpha C_\beta)$
959	−5	0	ethyl	938	3		2	943	942	941	941		ethyl, $\nu(C_\alpha C_\beta)$
927	8	3	$\nu(C_\alpha C_m)$, $\nu(C_\beta C_s)$	908	4	73	1	911	911	911	911	ν_{46}	ethyl, $\nu(C_\alpha C_m)$
								847	843	848			$\pi(C_m H)$
846	164	0	$\pi(C_m H)$	836	196	−4	0	840	837	843	843	γ_4, γ_{19}	$\pi(C_m H)$
834		0		823	16	−84	0	823	823	824	824	ν_{47}[c]	ethyl, $\pi(C_m H)$
								751	753				$\delta(C_\alpha C_m C_\alpha)$, ethyl
754	−12	0	π(skeletal)	747	−22	14	0	746	744	746	746		π(skeletal), ethyl
				741	−25	2	7	742	741	741	741	γ_5	π(skeletal)
742				737	−32	4	0			735	734	γ_{20}	π(skeletal)
726	0	4	$\nu(C_\alpha N)$	729	10	2	5	726		726		γ_{21}	π(skeletal)
								716	715	714	713		π(skeletal)
703	69	4	π(skeletal)	693	15		5	698	695			ν_{48}[c]	$\nu(C_\beta C_1)$, $\nu(C_\beta C_\beta)$, π(skeletal)
								688	686	691	689		π(skeletal)
605			$\nu(C_\alpha C_m)$, $\delta(C_\beta C_\beta C_s)$	596	5	34	0	596	594			ν_{51}[c]	$\delta(C_\beta C_\beta C_1)$, $\nu(C_\beta C_1)$, ethyl
								574	572				π(skeletal)
544				550	11	20	0	533	531	540	538	ν_{49}	π(skeletal)
				506	7	28	1	512	510	524	522	γ_{22}	π(skeletal), $\nu(C_\alpha C_m)$
								479	478	470	469	γ_6	π(skeletal)
				454	4	9	2	447	446	447	446	γ_{23}[c]	π(skeletal)
360				362	22	0	5	365	362	366	364	γ_7[c]	π(skeletal), $\pi(C_m H)$

[a] Kincaid, J. R.; Urban, M. W.; Watanabe, T.; Nakamoto, K. *J. Phys. Chem.* **1983**, *87*, 3096. [b] ν_i was assigned to a different frequency than that given by Li et al. in ref 3b but to the same frequency given by Kincaid et al. in ref 7. [c] ν_i was reassigned to a different frequency than that given in either Kincaid et al. in ref 7 or Li et al. in ref 3b. [d] ν_i was assigned to a different frequency than that given by Kincaid et al. in ref 7 but to the same frequency given by Li et al. in ref 3b.

1494 cm^{-1} upon meso-deuteration, whereas the 1483 cm^{-1} peak on the simulated spectrum shifts up to 1485 cm^{-1}. Similarly, the 959 cm^{-1} peak shifts up to 964 cm^{-1} on the experimental spectra, whereas the 938 cm^{-1} peak shifts down to 935 cm^{-1} on the simulated spectra. Where no shift is seen for the peak at 726 cm^{-1} (γ_{21}) on the experimental spectra, the simulated spectra show a shift from 729 to 719 cm^{-1}. The large shift of 69 cm^{-1} reported for the experimental peak at 703 cm^{-1} (ν_{48}) was not of the same magnitude in the simulated spectra: 693 to 678 cm^{-1}.

The shifts of the peaks at 1231, 1153, and 1133 cm^{-1} in the experimental natural abundance spectrum (ν_{42}, ν_{44}, and ν_{43}, respectively) and their counterparts for the simulated spectrum require explanation as a group. In their paper, Kincaid et al.[7] reported the following shifts: 1231 to 1185 cm^{-1}, 1153 to 948 cm^{-1}, and 1133 to 1151 cm^{-1}. Li and co-workers[3b] reported the experimental shifts differently: 1231 to 948 cm^{-1}, 1153 to 1185 cm^{-1}, and 1133 to 1151 cm^{-1}. For their calculated spectra, Li et al.[3b] reported the following shifts for these peaks: 1240 to 888 cm^{-1}, 1144 to 1212 cm^{-1}, and 1130 to 1129 cm^{-1}. Our analyses based on the total energy distribution for the internal coordinates for these vibrations indicate that for the simulated spectra the shifts are 1234 to 952 cm^{-1}, 1146 to 1144 cm^{-1}, and 1132 to 1184 cm^{-1}. The uncertainty about assigning this trio of peaks and their counterparts in the meso-d_4 spectra could be attributed to these vibrations being mixed. These three vibrations are comprised of many of the same components, and this may result in a mixing of modes among them.

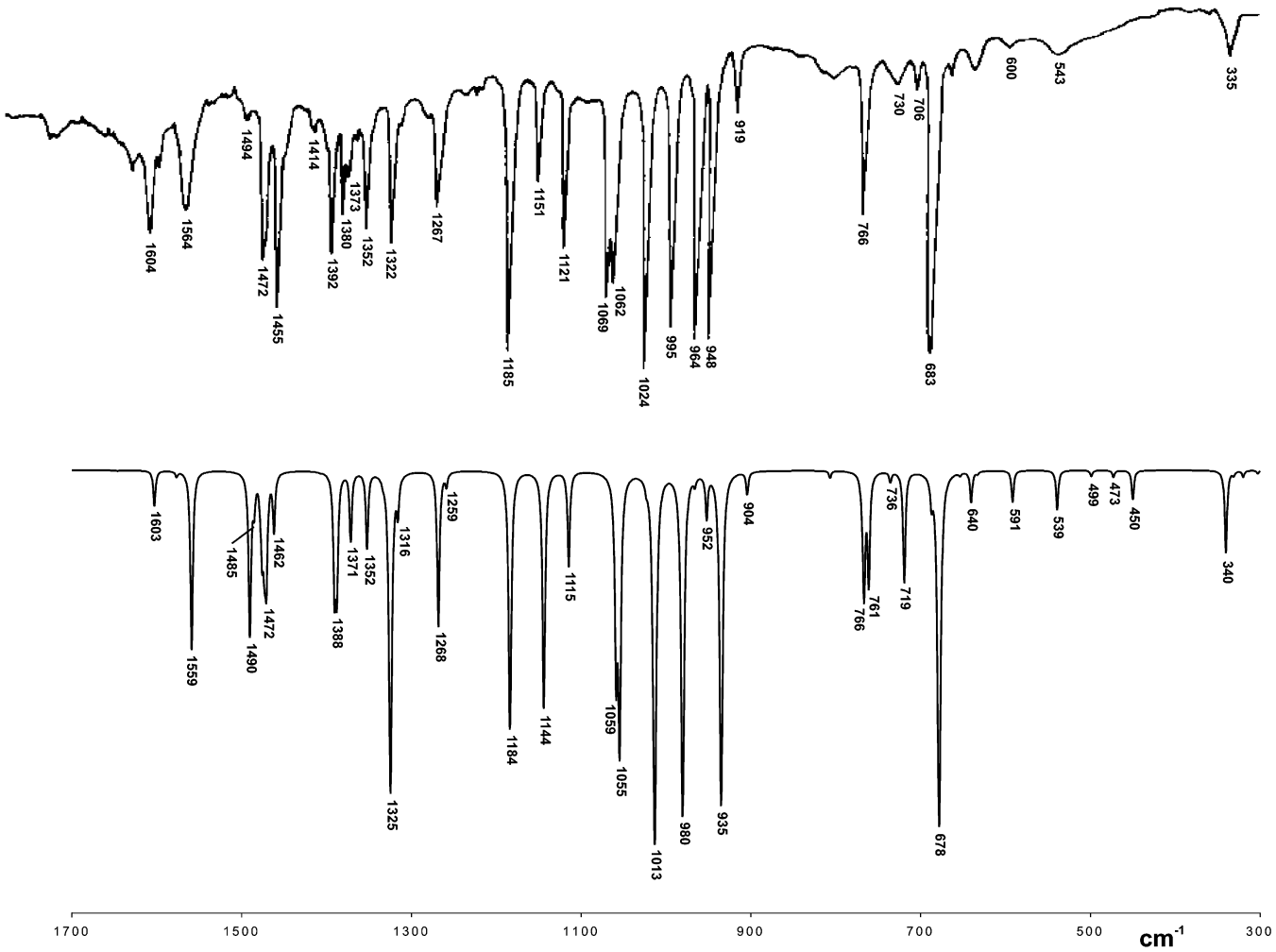

Figure 4. Comparison of experimental infrared spectrum (reproduced with permission from ref 7) with simulated spectrum (tetragonal conformer) for natural abundance NiOEP-d_4.

Regardless of how one matches the three natural abundance peaks (1231, 1153, and 1133 cm^{-1}) to the resulting peaks in the NiOEP-d_4 spectrum, there will be at least one peak with a negative shift value. Though deuteration results in the shifting of peaks to lower frequencies, meso-deuteration of the NiOEP macrocycle can, in fact, appear to result in the shift of a few of the peaks to higher wavenumbers. This can be attributed to a modes energy crossing due to kinematic coupling. In the simulated spectra, the shifts of larger negative values, with the exception of the previously discussed peak at 1132 cm^{-1}, are all associated with vibrations with a strong π(skeletal) component. This effect is also seen in the experimental spectra for the peak at 754 cm^{-1} and its corresponding shift of −12.

C. Isotopic Substitutions—Simulated Spectra. For comparison with the simulated natural abundance spectrum for the tetragonal conformer of NiOEP, three spectra representing various isotopic substitutions were created that correspond to incorporation of ^{15}N into the porphyrin macrocyle, deuteration at the four C_m atoms, NiOEP-d_4, and deuteration at the eight methylene carbons on the ethyl substituents, NiOEP-d_{16}. These spectra are presented in Figure 5, and the values for the resulting shifts are presented in Table 2.

The simulated Ni-^{15}N-OEP spectrum revealed shifts similar to those reported by Kincaid et al.[7] The shifts observed for the trio of peaks at 1234, 1146, and 1132 cm^{-1} (ν_{42}, ν_{44}, and ν_{43}) and for the peak at 983 cm^{-1} (ν_{45}) agree with the $\nu(C_\alpha N)$ component that is part of the assignments of each of these peaks. The peaks originally at 741 (γ_5), 729 (γ_{21}), 693 (ν_{48}), and 326 cm^{-1} (γ_7) shifted by 7, 5, 5, and 5 cm^{-1}, respectively, in keeping with their π(skeletal) components. The remaining peaks showing shifts in the Ni-^{15}N-OEP spectrum have either a π(skeletal) component or a stretching component involving the C_α atom, which would be affected by the close proximity of a heavy nitrogen atom.

Meso-deuteration of NiOEP results in very large shifts for two peaks: 1234 (ν_{42}) to 952 cm^{-1} and 836 (γ_4, γ_{19}) to 640 cm^{-1}. As explained previously, there is some ambiguity surrounding the assignment of the shifts to the three peaks 1234, 1146, and 1132 cm^{-1} (ν_{42}, ν_{44}, and ν_{43}, respectively) on the simulated natural abundance spectrum. Ambiguity aside, a shift of 282 for the peak at 1234 cm^{-1} in the natural abundance spectrum correlates with the fact that in-plane bending of the hydrogen at the C_m atom, $\delta(C_\alpha C_m H)$, comprises the largest portion of this vibration. Likewise a shift of 196 for the peak at 836 cm^{-1} (γ_4, γ_{19}) agrees with the assignment of this peak to the out-of-plane bending of the hydrogen on the meso-carbon atom, $\pi(C_m H)$.

Simulating a NiOEP-d_{16} spectrum yields large shifts for a number of peaks. The largest of these shifts belongs to peaks that have assignments comprised of only ethyl components (1462, 1324, 1316, 1277, and 1113 cm^{-1}). There are a number of vibrations that have assignments as only ethyl vibrations but

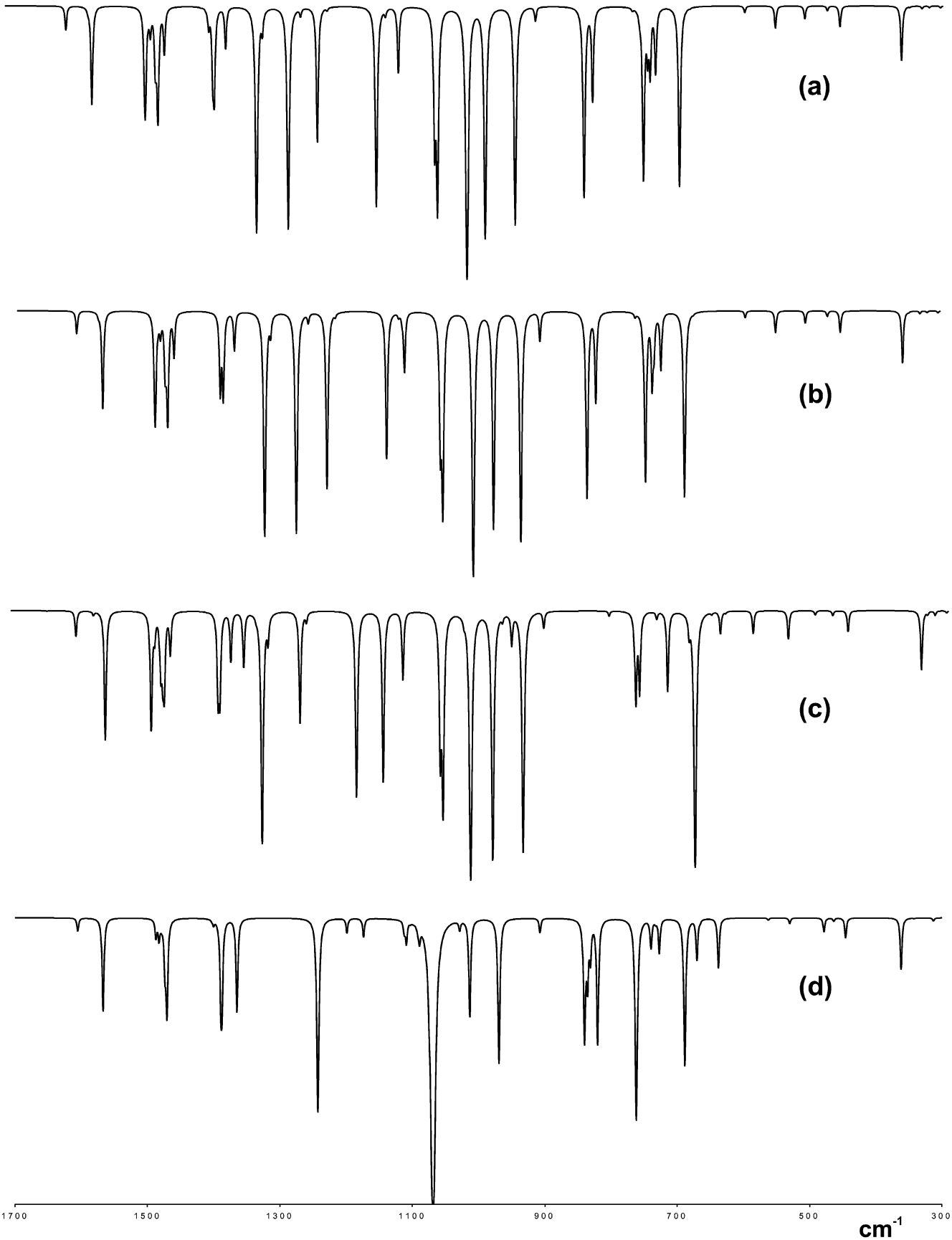

Figure 5. Comparison of simulated infrared spectra for NiOEP: (a) natural abundance with (b) ^{15}N, (c) meso-d_4, and (d) met-d_{16} isotopomers of tetragonal NiOEP.

do not show a large shift like the ones listed previously. In the convention used for describing vibrations in this paper, there is no distinction among the various types of ethyl vibrations. The peaks with strong ethyl components but little shift in the NiOEP-d_{16} spectrum correspond to vibrations involving the C_2 atom at the end of the ethyl substituents, such as bending of the hydrogen

atoms attached to C_2, that are affected little by deuteration at the methylene carbon atom, C_1. The three peaks that have large negative shifts, 1146 (ν_{44}), 1010, and 823 cm^{-1} (ν_{47}), are mixed vibrations comprised both of ethyl components and of other contributing vibrations. It is noted here that although Li and co-workers[3b] reported an experimental NiOEP-d_{16} spectrum, we have not compared our simulated values with this spectrum. The experimental NiOEP-d_{16} spectrum was obtained using KBr pellets, and the simulated spectra that we produced are best compared with experimental spectra obtained in an argon matrix.

D. Additional Observations. Simulated natural abundance spectra were created and compared for the tetragonal, ruffled triclinic A, and ruffled triclinic B conformers, and the frequencies for the peaks on these spectra are listed in Table 2. On the whole, these spectra show only a few subtle differences among the conformers. These spectra and discussion of the differences therein are available as Supporting Information. Likewise, the spectra of the planar and ruffled forms of the triclinic A and triclinic B conformers were compared for differences. There appears to be a few vibrations that show some sensitivity to ruffling of the macrocycle.

Conclusion

The simulated infrared spectra presented herein for NiOEP show remarkable agreement with the experimental spectra for NiOEP reported by Kincaid and co-workers.[7] The descriptions of the composition of each IR-active vibration obtained through analyses of density functional theory frequency calculation results also agreed in large part with those proposed by Kincaid et al.[7] in their experimental studies. Additionally, we report isotopic shifts similar to those obtained experimentally.

The comparison of simulated spectra for the various conformers of NiOEP revealed a handful of vibrations that appear to be sensitive to the orientation of the ethyl groups and a few that appear to be affected by the planarity of the macrocycle. The experimental natural abundance spectrum for NiOEP does not resemble exactly the spectrum of a single one of these conformers but instead exhibits characteristics that indicate a mixture of conformers was present in the experimental sample.

The successful simulation of theoretical infrared spectra that agree well with experimentally obtained spectra indicates that density functional theory frequency calculations may provide a useful tool for understanding further existing and future spectroscopic studies of metalloporphyrins. By using simulated spectra and the supporting information available for each vibration, future DFT studies may elucidate spectroscopic properties heretofore not fully understood.

Supporting Information Available: Simulated IR natural abundance spectra for nonplanar conformers of NiOEP and simulated IR spectra comparing planar and ruffled triclinic A and triclinic B conformers of NiOEP. This material is available free of charge via the Internet at http://pubs.acs.org.

References and Notes

(1) (a) Kitagawa, T.; Ozaki, Y. *Struct. Bonding* **1987**, *64*, 71. (b) Spiro, T. G.; Li, X. Y. In *Biological Applications of Raman Spectroscopy*; Spiro, T. G., Ed.; Wiley: New York, 1988; Vol. 3, p 1. (c) Spiro, T. G.; Czernuszewicz, R. S.; Li, X. Y. *Coord. Chem. Rev.* **1990**, *100*, 541. (d) Procyk, A. D.; Bocian, D. F. *Annu. Rev. Phys. Chem.* **1992**, *43*, 465.

(2) (a) Abe, M.; Kitagawa, T.; Kyoguku, Y. *J. Chem. Phys.* **1978**, *69*, 4526. (b) Kitagawa, T.; Abe, M.; Ogoshi, H. *J. Chem. Phys.* **1978**, *69*, 4516.

(3) (a) Li, X. Y.; Czernuszewicz, R. S.; Kincaid, J. R.; Su, Y. O.; Spiro, T. G. *J. Am. Chem. Soc.* **1990**, *94*, 31. (b) Li, X. Y.; Czernuszewicz, R. S.; Kincaid, J. R.; Stein, P.; Spiro, T. G. *J. Am. Chem. Soc.* **1990**, *94*, 47. (c) Li, X. Y.; Czernuszewicz, R. S.; Kincaid, J. R.; Spiro, T. G. *J. Am. Chem. Soc.* **1989**, *111*, 7012.

(4) (a) Hu, S.; Morris, I. K.; Singh, J. P.; Smith, K. M.; Spiro, T. G. *J. Am. Chem. Soc.* **1993**, *115*, 12446. (b) Hu, S.; Smith, K. M.; Spiro, T. G. *J. Am. Chem. Soc.* **1996**, *118*, 12638.

(5) (a) Kozlowski, P. M.; Rush, T. S.; Jarzecki, A. A.; Zgierski, M. Z.; Chase, B.; Piffat, C.; Ye, B.-H.; Li, X.-Y.; Pulay, P.; Spiro, T. G. *J. Phys. Chem. A* **1999**, *103*, 1357. (b) Rush, T. S.; Kozlowski, P. M.; Piffat, C. A.; Kumble, R.; Zgierski, M. Z.; Spiro, T. G. *J. Phys. Chem. B* **2000**, *104*, 5020.

(6) Stoll, L. K.; Zgierski, M. Z.; Kozlowski, P. M. *J. Phys. Chem. A* **2002**, *106* (1), 170.

(7) Kincaid, J. R.; Urban, M. W.; Watanabe, T.; Nakamoto, K. *J. Phys. Chem.* **1983**, *87*, 3096.

(8) Stoll, L. K.; Czader, A.; Zgierski, M. Z.; Czernuszewicz, R. S.; Kozlowski, P. M. Unpublished results.

(9) Frisch, M. J.; Trucks, G. W.; Schlegel, H. B.; Scuseria, G. E.; Robb, M. A.; Cheeseman, J. R.; Zakrzewski, V. G.; Montgomery, J. A., Jr.; Stratmann, R. E.; Burant, J. C.; Dapprich, S.; Millam, J. M.; Daniels, A. D.; Kudin, K. N.; Strain, M. C.; Farkas, O.; Tomasi, J.; Barone, V.; Cossi, M.; Cammi, R.; Mennucci, B.; Pomelli, C.; Adamo, C.; Clifford, S.; Ochterski, J.; Petersson, G. A.; Ayala, P. Y.; Cui, Q.; Morokuma, K.; Malick, D. K.; Rabuck, A. D.; Raghavachari, K.; Foresman, J. B.; Cioslowski, J.; Ortiz, J. V.; Stefanov, B. B.; Liu, G.; Liashenko, A.; Piskorz, P.; Komaromi, I.; Gomperts, R.; Martin, R. L.; Fox, D. J.; Keith, T.; Al-Laham, M. A.; Peng, C. Y.; Nanayakkara, A.; Gonzalez, C.; Challacombe, M.; Gill, P. M. W.; Johnson, B. G.; Chen, W.; Wong, M. W.; Andres, J. L.; Head-Gordon, M.; Replogle, E. S.; Pople, J. A. *Gaussian 98*, revision A.3; Gaussian, Inc.: Pittsburgh, PA, 1998.

(10) Schäfer, A.; Horn, H.; Ahlrichs, R. *J. Phys. Chem.* **1992**, *97*, 2571.

(11) (a) Kozlowski, P. M.; Spiro, T. G.; Berces, A.; Zgierski, M. Z. *J. Phys. Chem. B* **1998**, *102*, 2603. (b) Spiro, T. G.; Kozlowski, P. M. *J. Am. Chem. Soc.* **1998**, *120*, 4524. (c) Spiro, T. G.; Kozlowski, P. M. *J. Raman Spectrosc.* **1998**, *29*, 869.

(12) Fogarasi, G.; Zhou, X.; Taylor, R. W.; Pulay, P. *J. Am. Chem. Soc.* **1992**, *114*, 8191.

(13) Pulay, P. *TX90*; Fayetteville, AR, 1990. Pulay, P. *Theor. Chim. Acta* **1979**, *50*, 229.

(14) (a) Pulay, P.; Fogarasi, G.; Pongor, G.; Boggs, J. E.; Vargha, A. *J. Am. Chem. Soc.* **1983**, *105*, 7037. (b) Rauhut, G.; Pulay, P. *J. Phys. Chem.* **1995**, *99*, 3093. (c) Kozlowski, P. M.; Zgierski, M. Z.; Pulay, P. *Chem. Phys. Lett.* **1995**, *247*, 379. (d) Kozlowski, P. M.; Jarzecki, A. A.; Pulay, P.; Li, X.-Y.; Zgierski, M. Z. *J. Phys. Chem.* **1996**, *100*, 13985.

(15) Flükiger, P.; Lüthi, H. P.; Portmann, S.; Weber, J. *MOLEKEL 4.0*; Swiss Center for Scientific Computing: Manno, Switzerland, 2000.

(16) Kincaid, J. R. Personal communication.